

# Simulating a direct shear box test by DEM

S.H. Liu

**Abstract:** Distinct element simulation was performed for direct shear box (DSB) tests on a dense and a loose two-dimensional (2D) sample of 3259 cylinders. Special attention was devoted to the effect that the frictional force between the inside surface of the upper shear box and the sample had on the measured shear strength in the DSB test. Some ways of minimizing this interface frictional force were introduced in the paper. Given that the deformation approximates simple shear within the deforming zone across the sample centre (referred to as the shear zone), a method was proposed to evaluate the overall strains in the DSB test. The numerically simulated data were used to interpret, on a microscopic scale, the angle of internal friction and a 2D stress–dilatancy equation for the mobilized plane in granular material. It was found that the angle of internal friction in granular material is not directly related to the interparticle friction angle ( $\phi_\mu$ ). Instead, it relates to the average interparticle contact angle ( $\bar{\theta}$ ) on the mobilized plane and the ratio  $k/f_0$ , representing the degree of the probability distribution of the interparticle contact forces that is biased toward the positive zone of the contact angle  $\theta$  (along the shear direction), where  $k$  is the slope of the linear distribution of the average interparticle contact forces against the interparticle contact angle; and  $f_0$  is the average interparticle contact force.

*Key words:* angle of internal friction, direct shear box test, distinct element method, friction, granular material, stress–dilatancy.

**Résumé :** On a réalisé une simulation en éléments distincts pour les essais à la boîte de cisaillement direct (à laquelle l'abréviation DSB est attribuée dans cet article) sur un échantillon 2D dense et lâche de 3 259 cylindres. On a accordé une attention particulière à l'effet de la force de frottement entre l'échantillon et la surface intérieure de la partie supérieure de la boîte de cisaillement sur la résistance au cisaillement mesurée dans l'essai DSB. On a introduit dans cet article des façons de minimiser la force de frottement à l'interface. Considérant que la déformation est proche du cisaillement simple à l'intérieur de la zone en déformation au centre de l'échantillon (soit la zone de cisaillement), on a proposé une méthode pour évaluer les déformations globales dans l'essai DSB. Au moyen des données numériques simulées, l'angle de frottement interne et l'équation de contrainte de dilatance bidimensionnelle sur le plan mobilisé pour un matériau granulaire ont été interprétés à l'échelle microscopique. On a trouvé que l'angle de frottement interne du matériau granulaire n'est pas en relation directe avec l'angle de frottement interparticule  $\phi_\mu$ . Il est plutôt en relation avec l'angle moyen de contact interparticule  $\bar{\theta}$  sur le plan mobilisé et le rapport  $k/f_0$  représentant la distribution de la probabilité des forces de contact interparticule tendant vers la zone positive de l'angle de contact  $\theta$  (le long de la direction du cisaillement), où  $k$  est la pente de la distribution linéaire de la moyenne des forces de contact interparticule par rapport à l'angle de contact interparticule, et  $f_0$  est la force moyenne de contact interparticule.

*Mots clés :* angle de frottement interne, essai de cisaillement direct, méthode d'éléments distincts, frottement, matériau pulvérulent, contrainte–dilatance.

[Traduit par la Rédaction]

## Introduction

The testing of soils by applying a shear load (or displacement) has resulted in a worldwide revival of interest over the last few decades. Several types of laboratory device have been developed for directly determining the shear strength envelope for soils. Among them, the direct shear box (DSB) test, with both an upper shear box and a lower one, has most commonly been used, because the testing procedures are simple, and it is capable of approximately simulating the deformation conditions of plane strain as occurs in many field

problems. In the conventional DSB test, shearing of the sample is often achieved by pushing the lower shear box horizontally while the upper shear box is restrained vertically and horizontally (Taylor 1948; Skempton and Bishop 1950), as shown in Fig. 1. The shear force is measured with a bearing ring or a load cell that is attached to the upper shear box. In this DSB device, a frictional force is generated at the attachment point when the upper shear box moves up or down as a result of the volume change in the sheared sample (dilation or contraction). Sometimes, to prevent tilting of the upper shear box during the shearing process, a clasp is set opposite the attachment point. In turn, the frictional force at the attachment point and the clasp restrain the upward or downward movement of the upper shear box. Consequently, a frictional force between the inside surface of the upper shear box and the sample is generated when the volume of the sheared sample changes (dilation or contraction). Owing to this frictional force at the shear box – sam-

Received 4 February 2004. Accepted 19 October 2005.  
Published on the NRC Research Press Web site at  
<http://cgj.nrc.ca> on 26 January 2006.

**S.H. Liu.** College of Water Conservancy and Hydropower Engineering, Hohai University, Xikang Road 1, Nanjing 210098, PR China (e-mail: [sihong\\_hhu@yahoo.com.cn](mailto:sihong_hhu@yahoo.com.cn)).

Fig. 1. Schematic of conventional direct shear box test device

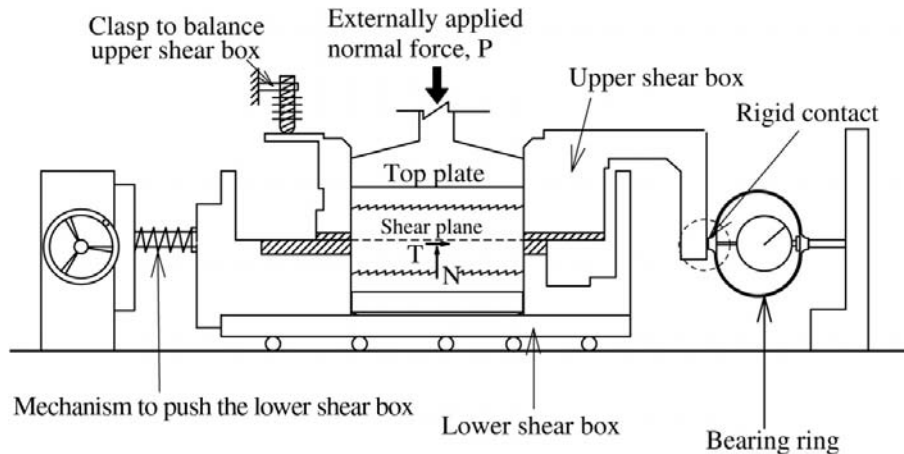
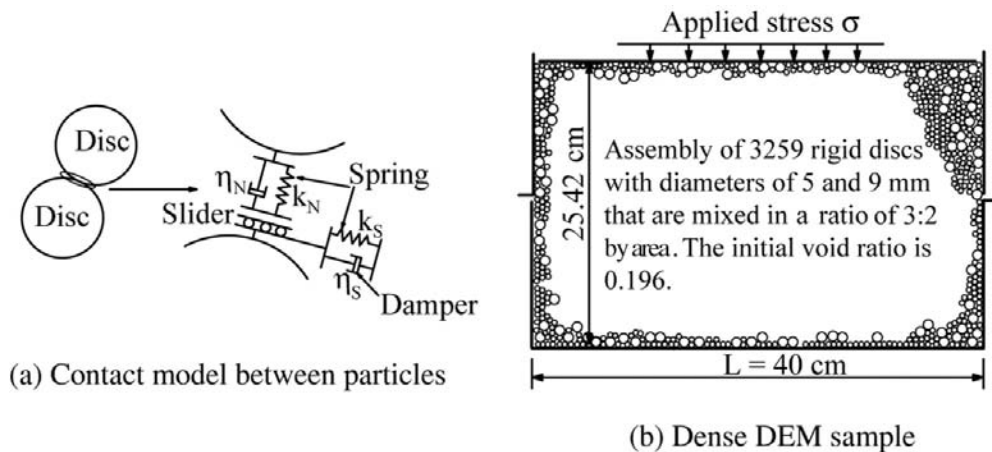


Fig. 2. Simulation of direct shear test: (a) DEM contact model; (b) box description.



ple interface, the shear strength is generally overestimated for dilatant specimens (like coarse granular soils) but underestimated for contractive specimens in the DSB tests, as reported by Takada et al. (1996) and Sumi et al. (1997). Moreover, the DSB test is inevitably subject to such criticisms as the full stress and strain states are not defined; and only the horizontal shear stress ( $\tau_{zx}$ ) and the vertical stress ( $\sigma_z$ ) are available. The strains cannot be obtained from the measured horizontal (shear) displacement ( $D$ ) and the vertical displacement ( $h$ ) because of the nonuniformity of the deformation throughout the sample in the DSB test. For this reason, difficulties arise in understanding the relationship between parameters derived from the DSB test and those derived from other laboratory and field testing devices.

In this paper, distinct element simulation is performed for the DSB test for better understanding of the intrinsic drawbacks in this test, since it can provide microscopic information that is difficult to obtain experimentally, such as particle displacements and the particle-particle contact force network. The possible ways to remove or minimize the frictional force at the internal surface of the upper shear box are then introduced. On the basis of the numerically simulated results, a method to evaluate strains in the DSB test is proposed. Furthermore, the angle of internal friction and a

stress-dilatancy relationship for granular material are interpreted on the microscopic scale.

## Discrete modeling of the direct shear box test

### Distinct element method

The discrete method used is the distinct element method (DEM) pioneered by Cundall (1971) and Cundall and Strack (1979). The DEM is a numerical technique that keeps track of the motion of individual particles and updates any contact with neighboring elements by using a constitutive contact law. In two dimensions (2D) each particle has three degrees of freedom (two translations and one rotation). Each particle can be in contact with neighboring particles or boundaries. In the present work, the DEM program used is GRADIA (Yamamoto 1995). The particles in GRADIA are circular; their mechanical interaction is characterized by using the so-called soft contact approach. In this approach, although the particles are assumed to be rigid for the purposes of shape definition, elastic deformation is allowed to take place at the contacts. The constitutive contact model used in GRADIA is shown in Fig. 2a. It consists of two parts: (1) a stiffness model providing a linear elastic relation between the contact

**Table 1.** Input parameters for numerical simulation by DEM.

	Particle–particle	Particle–wall
Normal stiffness, $k_N, k'_N$ ( $\text{N m}^{-1} \text{m}^{-1}$ )	$5.0 \times 10^9$	$9.0 \times 10^9$
Shear stiffness, $k_S, k'_S$ ( $\text{N m}^{-1} \text{m}^{-1}$ )	$1.5 \times 10^8$	$3.0 \times 10^8$
Normal damping, $\eta_N, \eta'_N$ ( $\text{N s m}^{-1} \text{m}^{-1}$ )	$5.56 \times 10^4$	$7.8 \times 10^4$
Shear damping, $\eta_S, \eta'_S$ ( $\text{N s m}^{-1} \text{m}^{-1}$ )	$0.99 \times 10^4$	$1.4 \times 10^4$
Interparticle friction angle, $\phi_\mu, \phi'_\mu$ ( $^\circ$ )	16	16
Density of particles, $\rho$ ( $\text{kg m}^{-3}$ )	2700	
Time increment, $\Delta t$ (s)	$5 \times 10^{-7}$	

force and the contact relative displacement in the normal and shear directions; and (2) a slip model enforcing a Coulomb-type relation between the shear and normal contact forces. Because of the dynamic formation of the model, energy dissipation through frictional sliding may not be sufficient for a steady-state solution. Additional dissipation is achieved by small amounts of viscous damping. The forces generated at a contact are computed on the basis of the overlap of the bodies at the contact and the stiffness of the springs. The forces from all the contacts on a single body are summed, yielding a resultant force, which is then used to compute the acceleration of the body according to Newton's second law of motion. After the acceleration is determined, the new velocity and displacement of the particle are computed by using central difference explicit time integration. With the newly computed displacement configuration, the state of deformation at existing contacts is reevaluated, and the possible creation of new contacts is evaluated, leading to a new cycle of computation.

### Simulation process

The initial state of the DEM sample is created by random deposition under gravity of circular particles into a shear box with a unit thickness. The DEM sample consists of circular particles having binary diameters of 5 and 9 mm that are mixed in a ratio of 3:2 by area, simulating an assembly of aluminum rods that I had used in experimental tests. To investigate the difference between the frictional force produced on the inside surface of the upper shear box by dilatant behavior of the specimens and that produced by contractive behavior, two distinct initial states with void ratios of  $e_0 = 0.196$  and  $0.233$  are generated. The looser initial state ( $e_0 = 0.233$ ) is obtained by following the above deposition procedure and using the particle–particle friction angles of  $\phi_\mu = 16^\circ$ , whereas the denser one ( $e_0 = 0.196$ ) is the result of the same procedure but using  $\phi_\mu = 0^\circ$ . The particle deposition under  $\phi_\mu = 0^\circ$  is a numerical technique to create a denser sample, as used by some researchers (e.g., Thornton 2000; Masson and Martinez 2001). The particle–particle friction angle,  $\phi_\mu = 16^\circ$ , is introduced after the deposition under  $\phi_\mu = 0^\circ$ , just before the beginning of the shearing action. The denser DEM sample has 3259 particles, contained in a shear box 40 cm wide  $\times$  25.42 cm high (Fig. 2b); the looser DEM sample has the same number of particles, but they are contained in a slightly higher shear box, which is 40 cm wide  $\times$  26.21 cm high. As shown in Fig. 1, in the conventional DSB test the upper shear box is usually constricted vertically with a clasp to prevent it from rotating, and it is attached horizontally to a bearing ring or load cell for mea-

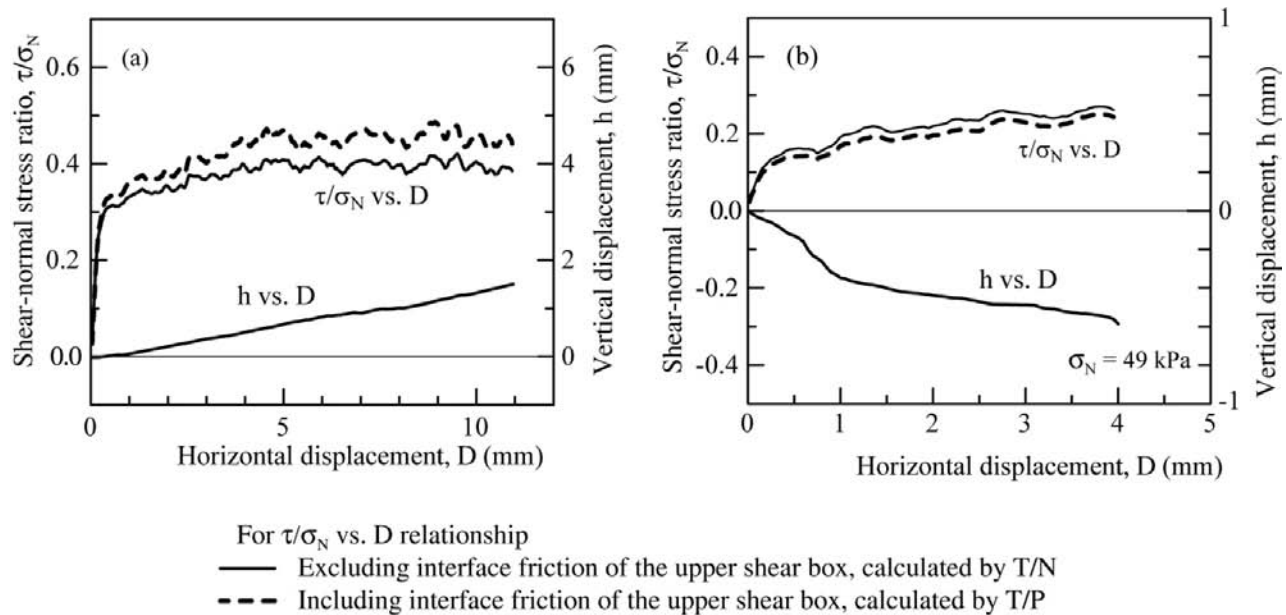
suring the shear force, which causes the upper shear box to remain almost stationary during the shearing process. Thus, in the simulation, the upper shear box approximates a fixed position in both vertical and horizontal directions. The particles are sheared by the lower shear box moving horizontally at a speed of  $0.5 \text{ cm s}^{-1}$  under the application of a constant vertical stress of  $\sigma = 49 \text{ kPa}$  on the top plate of unit thickness.

The input parameters used in our simulation are summarized in Table 1 and correspond to the properties of aluminum. The normal and shear stiffness ( $k_N, k_S$ ) and damping ( $\eta_N, \eta_S$ ) in Table 1 are based on the contact theory of two elastic discs and consider the level of stress possibly applied to the granular sample. The interparticle friction angle ( $\phi_\mu = 16^\circ$ ) is obtained from the frictional tests on aluminum rods. The time step  $\Delta t$  is chosen to be 1/10 of the critical time step  $\Delta t_c$  in order to maintain a quasi-static state during the calculation, where  $\Delta t_c = 2(m/k)^{1/2}$ , which is based on the single degree-of-freedom system of a mass  $m$  connected to the ground by a spring of stiffness  $k$ .

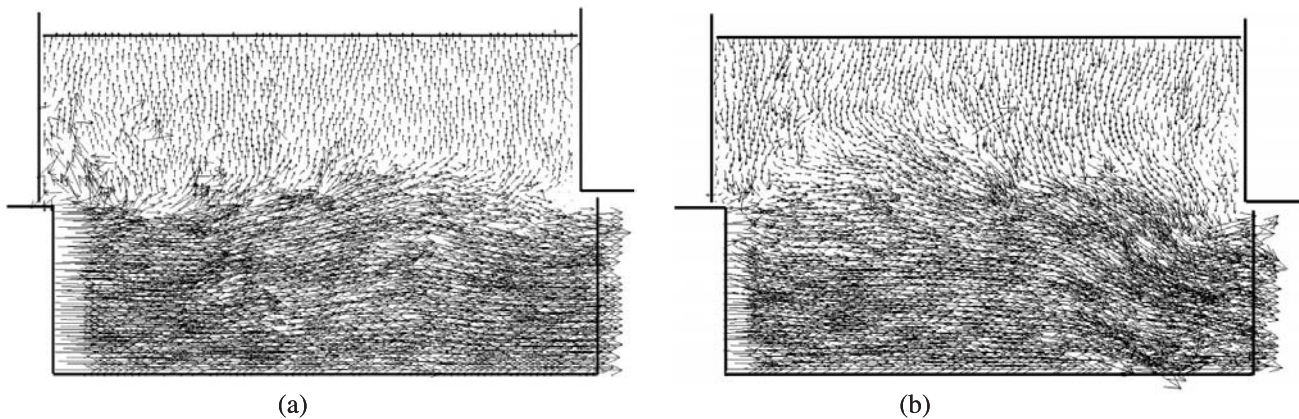
### Simulation results focusing on the interface friction inside the upper shear box

Figure 3 shows the simulation results in terms of macroscopic behavior for the two initial densities. The macroscopic shear stress to normal stress ratio ( $\tau/\sigma_N$ ) is calculated separately through  $T/N$  and  $T/P$ , where  $P$  is the applied normal force on the top plate; and  $T$  and  $N$  are the shear and normal forces on the split plane (shear plane), which are deduced from the static equilibrium of the lower half sample by summing the horizontal and vertical forces acting on its boundaries (vertical walls and bottom plate), respectively. Clearly,  $T/N$  is the true stress ratio for the shear plane excluding the effect of the interface frictional forces inside the upper shear box, whereas  $T/P$  is the stress ratio equivalent to the one measured from the usual tests involving the interface frictional forces inside the upper shear box. The vertical displacement ( $h$ ) is obtained from the vertical displacement of the top plate, representing the overall volume change. It is seen from Fig. 3a that the denser sample exhibits a very stiff response at the beginning of shear. As a typical response of dense assemblies, the volume increase observed during shear characterizes dilatant behavior. Shearing of the loose sample (see Fig. 3b) is produced with a lower rate of shear stress increase than is shearing of the dense sample, which clearly leads to a softer macro-shear modulus. The change in volume of the loose sample corresponds to contractive behavior. Thus, these simulations provide macroscopic behaviors that are representative of dense and loose granular materials.

**Fig. 3.** Numerically simulated evolution of shear stress to normal stress ratio and volume change for the conventional direct shear box tests: (a) dense sample; (b) loose sample.



**Fig. 4.** Particle instantaneous velocity field: (a) dense sample; (b) loose sample.



Moreover, it can be seen that the stress ratio  $\tau/\sigma_N$  calculated by  $T/N$  is smaller than that calculated by  $T/P$  for the dense sample and vice versa for the loose sample.

Figure 4 shows the instantaneous velocity field of the particles within the granular specimens. It can be observed that for both the dense and the loose samples, particles in the lower shear box displace horizontally in general. However, for the dense sample, particles in the upper shear box are driven by an upward motion due to dilation (Fig. 4a), whereas for the loose sample, particle motion velocities are downward, corresponding to sample contraction (Fig. 4b).

Figure 5 shows the networks of contact forces corresponding to the shear displacements of  $D = 7$  mm for the dense sample and  $D = 4$  mm for the loose sample, with details of the transmission of forces between the vertical walls of the upper shear box and the boundary particles. It is seen that the resultant frictional force beside the vertical walls of the upper shear box is downward for the dense sample because of dilation, whereas it is upward for the loose sample because of contraction. For the dense sample, the downward

interface friction force leads to  $N > P$  and in turn  $T/N < T/P$  (see Fig. 1). In contrast, the contractive behavior of the loose sample results in  $T/N > T/P$ . This scenario correlates well with the experimental observations that the shear strength obtained from the conventional DSB test is usually overestimated for dilatant specimens but underestimated for contractive ones.

The inside-wall frictional force of the upper shear box can be minimized or even eliminated if the upper shear box is allowed to move freely in the vertical direction. Figure 6 presents a possible way to do this: smooth Teflon rods and a Teflon plate (the coefficient of friction for Teflon is about 0.02) are inserted between the upper shear box and the bearing ring, and the clasp is eliminated (Matsuoka et al. 2001). To prevent the top plate from jamming within the upper shear box if either the upper shear box or the top plate tilts during shear, the top plate (loading plate) is lifted up to the rim of the upper shear box. Figure 7 shows the simulation results of the modified DSB tests on the same two dense and loose DEM samples. It can be seen that the evolution of the

Fig. 5. Particle–particle and particle–wall contact forces network: (a) dense sample; (b) loose sample.

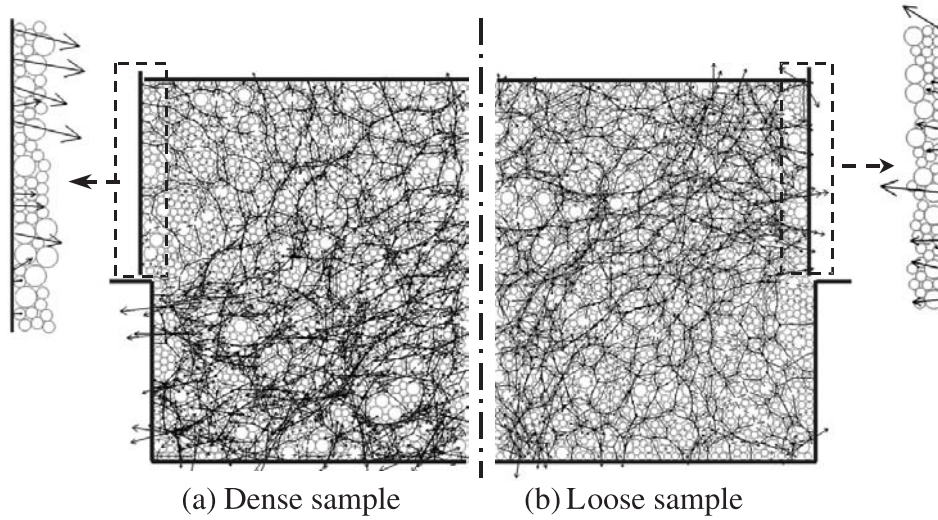


Fig. 6. Conventional direct shear box improved with low-friction Teflon rods and Teflon platen.

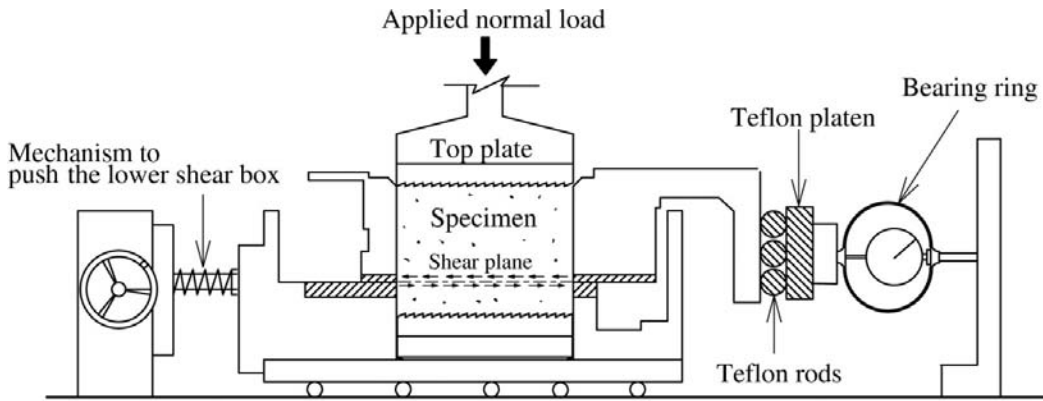


Fig. 7. Numerically simulated evolution of shear stress to normal stress ratio and volume change for the improved direct shear box tests: (a) dense sample; (b) loose sample.

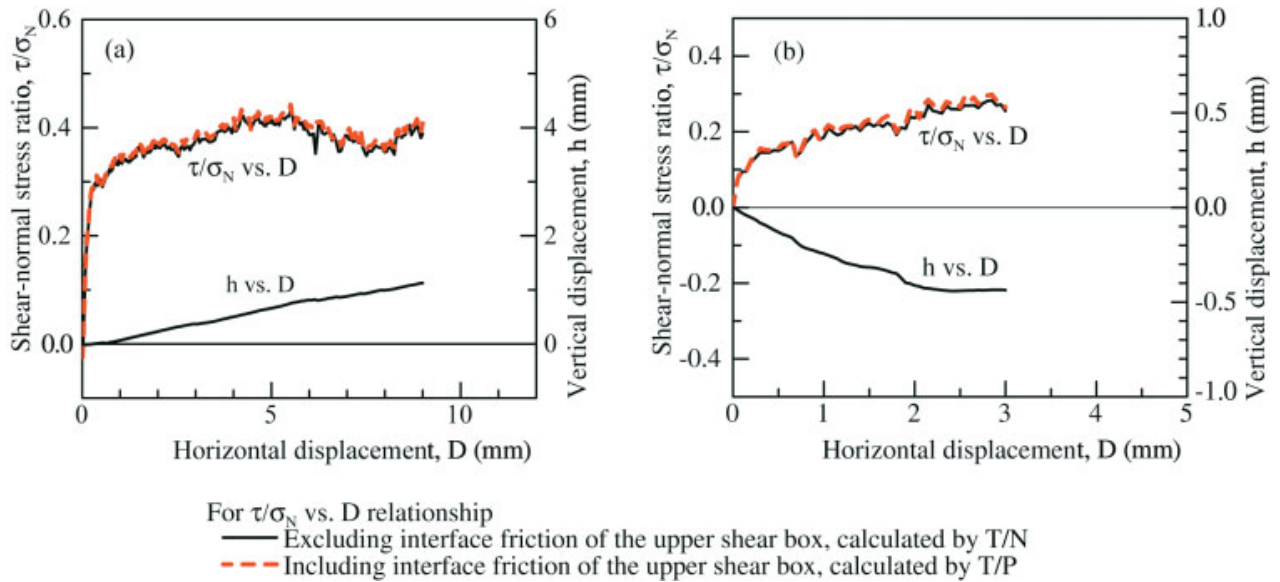


Fig. 8. Simple shear mode of deformation in the central part of the direct shear box test.

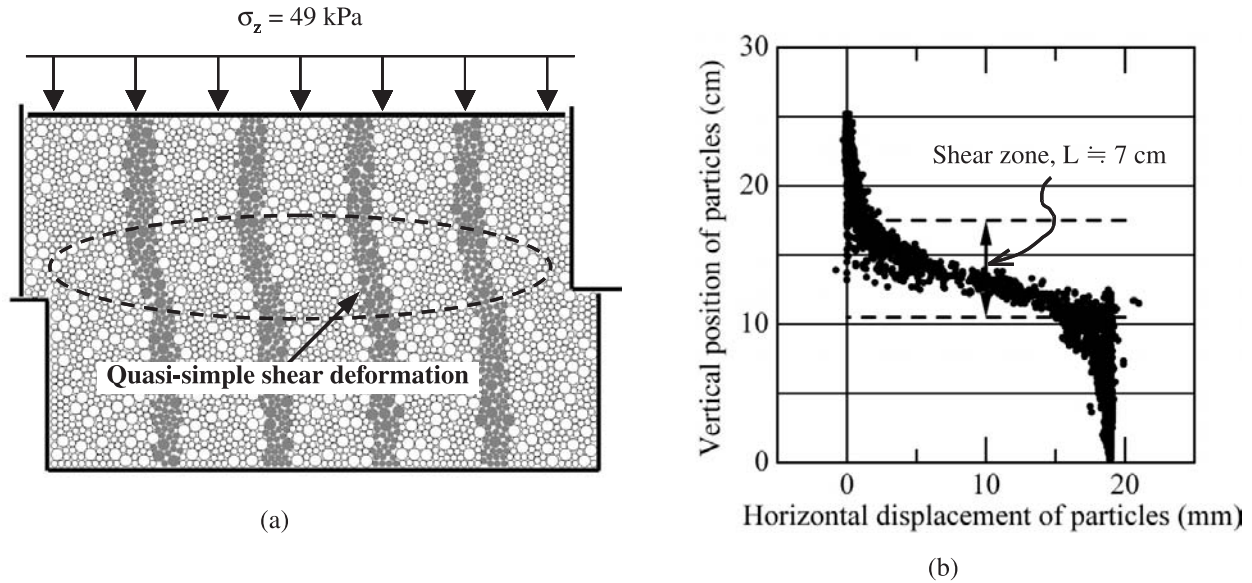
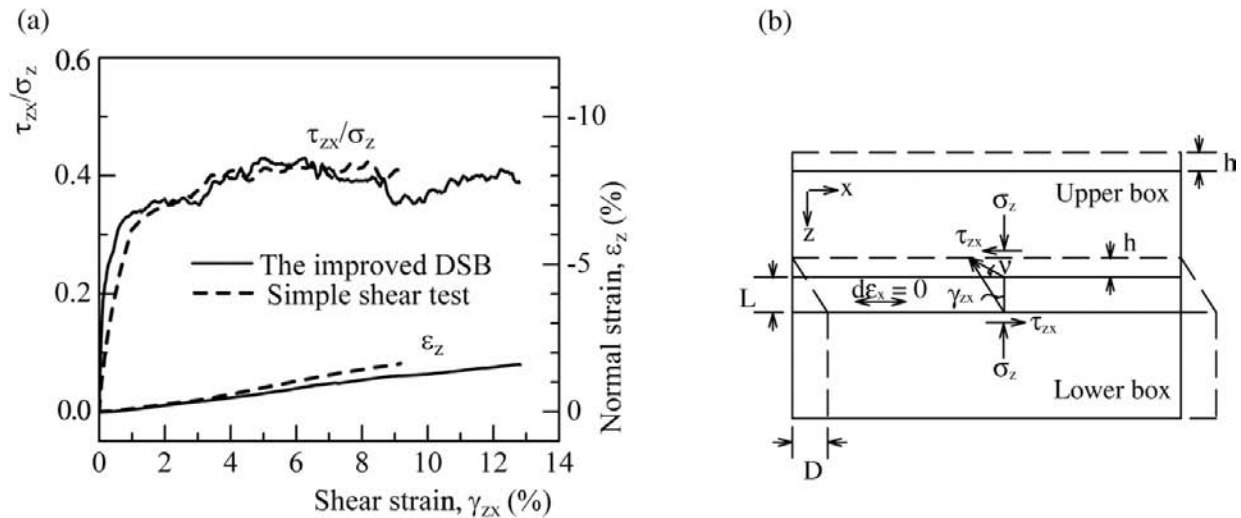


Fig. 9. (a) Comparison of the simulated stress–strain relationships of direct shear box (DSB) and simple shear tests on the horizontal plane; (b) simple shear mode of deformation assumed in DSB test.



shear stress to normal stress ratios determined by  $T/N$  agrees quite well with that determined by  $T/P$  for the dense and loose samples, indicating the effectiveness of the proposed method for reducing the inside-wall frictional force of the upper shear box.

In the above discrete simulations, the normal force ( $N$ ) on the shear plane is deduced from the resultant vertical forces (along the gravity direction) on all boundaries of the lower shear box, thanks to the static equilibrium in the gravity direction. This suggests that the true normal force ( $N$ ) on the shear plane can be equivalently and accurately measured on the opposite side of the loading plate. It is worthwhile mentioning that this technique has been adopted as a standard for the DSB test by the Japanese Geotechnical Society (1997).

**Strain evaluation in direct shear box test**

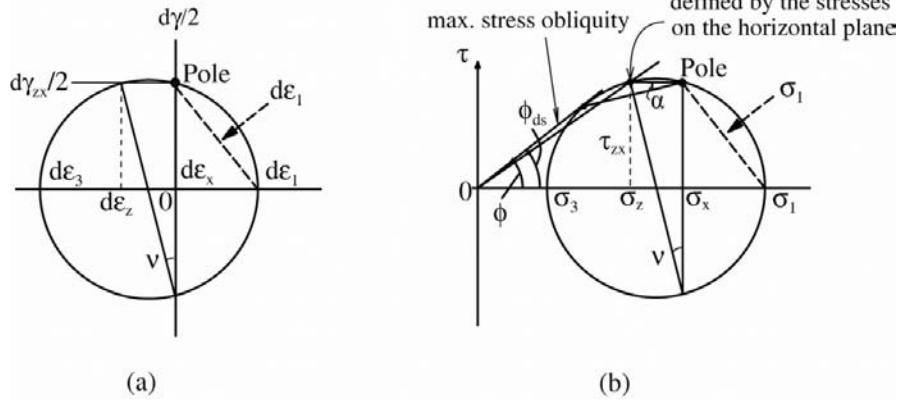
In DSB tests, the full strain state is not defined, because the deformations throughout the sample are not uniform. In-

formation is available only on the horizontal (shear) displacement ( $D$ ) and the vertical displacement ( $h$ ). These intrinsic drawbacks make the proper interpretation of the DSB test difficult. However, as revealed by the DEM simulation (Fig. 8) (also see Thornton and Zhang 2001), the shear deformation in the central region of the sample is relatively uniform, exhibiting nearly simple shear. Such a region, with uniform shear deformation, is commonly called the shear zone, or shear band. The thickness ( $L$ ) of the shear zone in Fig. 8 is about 7 cm, that is, 10 times the average grain size of the DEM sample. Given the thickness ( $L$ ) of the shear zone, the shear strain ( $\gamma_{zx}$ ) and the normal strain ( $\epsilon_z$ ) on the horizontal plane can be estimated by

$$[1] \quad \gamma_{zx} = D/L, \quad \epsilon_z = h/L$$

representing the overall degree of shearing in the DSB test. Figure 9a compares the stress–strain curves of the DSB test corresponding to Fig. 7a, where the strains are calculated

**Fig. 10.** Mohr circles of strain increments and stress in direct shear and simple shear tests.



with eq. [1], using  $L = 7$  cm, with those from the simple shear test (SST) using the same particle composition (Liu and Matsuoka 2001, 2003). The good agreement between those two test results supports the assumption that each element of the sample in the DSB test undergoes a simple shear deformation within the shear zone, as schematically depicted in Fig. 9b. Thus, if the thickness of the shear zone is properly determined, the overall strains in the DSB test can be defined.

In the idealized simple shear mode of deformation, the length of the sample remains constant during shear, leading to a zero horizontal strain increment, that is,  $dε_x = 0$ . As a result, the principal strain increments ( $dε_1, dε_3$ ) in the DSB test can be obtained from Mohr's circle of incremental strain (Fig. 10a) (Bolton 1986; Shibuya et al. 1997; Lings and Dietz 2004):

$$[2a] \quad dε_1 = dε_z + \left( \frac{\sin v + 1}{\cos v} \right) \frac{dγ_{zx}}{2}$$

$$[2b] \quad dε_3 = dε_z + \left( \frac{\sin v - 1}{\cos v} \right) \frac{dγ_{zx}}{2}$$

where the increments of the shear strain ( $dγ_{zx}$ ) and the normal strain ( $dε_z$ ) on the horizontal plane are estimated from eq. [1]. The angle of dilation ( $v$ ) (see Fig. 9b) is obtained from the rate of change of vertical displacement ( $h$ ) (compression is taken as positive) with horizontal displacement ( $D$ ):

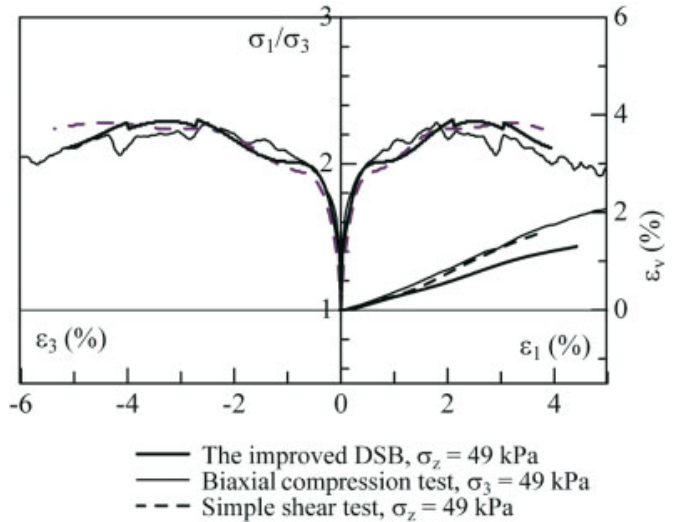
$$[3] \quad v = \tan^{-1} (-dε_z/dγ_{zx}) = \tan^{-1} (-dh/dD)$$

which assumes that all dilation occurs within the simple shear zone of thickness  $L$ . The 2D volumetric strain is given by

$$[4] \quad dε_v = dε_1 + dε_3$$

To verify the above strain evaluation method for the DSB test through comparisons with the biaxial compression test, the principal stresses in the DSB test need to be determined as well. Experiments by, for example, Cole (1967) and Dyer (1986) have shown that at peak state, the principal axes of stress and incremental strain coincide in the idealized simple shear mode of deformation. This coaxiality is assumed to be true as well during the pre-peak simple shear deformation. Under this assumption and the condition of zero horizontal strain increment, the principal stresses ( $σ_1$  and  $σ_3$ ) in the

**Fig. 11.** Comparison of the numerically simulated results of direct shear box, biaxial compression, and simple shear tests in terms of the principal stress–strain relation.



simple shear deformation are given by the following (see Fig. 10):

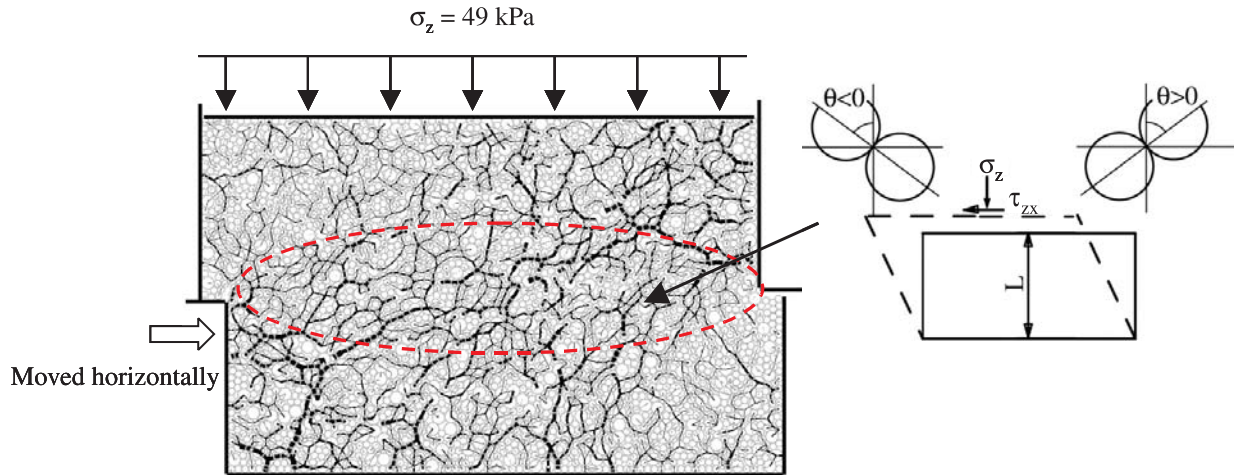
$$[5a] \quad σ_1 = σ_z + \left( \frac{\sin v + 1}{\cos v} \right) τ_{zx}$$

$$[5b] \quad σ_3 = σ_z + \left( \frac{\sin v - 1}{\cos v} \right) τ_{zx}$$

where  $σ_z$  is the average vertical stress ( $= P/A$ , where  $A$  is the cross-sectional area of the sample); and  $τ_{zx}$  is the average shear stress ( $= T/A$ ). Figure 11 compares the principal stress–strain relationships for the DSB test and SST corresponding to Fig. 9a with those of the numerically simulated biaxial compression test using a similar particle composition (Liu 1999; Matsuoka et al. 1999). The good agreement of the principal stress–strain curves from these three types of tests indicates the reasonableness of the proposed strain evaluation for DSB tests.

It is noted that the principal strain increments ( $dε_1$  and  $dε_3$ ) calculated by eq. [2] are in 2D form. For DSB tests on field soils, however, the principal strain increments should be converted into three-dimensional (3D) ones so that they

Fig. 12. Interparticle contact forces network in the simulated direct shear box test.



can be compared with the results of triaxial compression tests. For this purpose, the concept of compounded mobilized planes (CMPs), proposed by Matsuoka (1974, 1983), is used. Based on the CMP concept, the principal strain increments under triaxial compression conditions ( $d\epsilon_1^{3D}$  and  $d\epsilon_2^{3D} = d\epsilon_3^{3D}$ ), are given

$$[6a] \quad d\epsilon_1^{3D} = 2d\epsilon_1$$

$$[6b] \quad d\epsilon_2^{3D} = d\epsilon_3^{3D} = d\epsilon_3$$

$$[6c] \quad d\epsilon_v = d\epsilon_1^{3D} + 2d\epsilon_3^{3D}$$

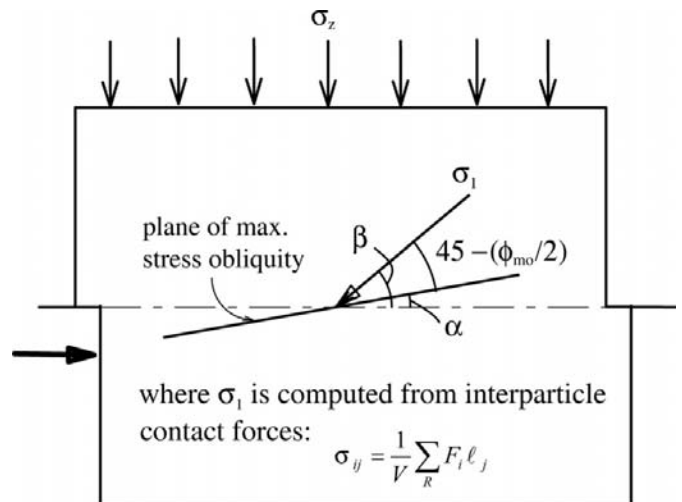
The above strain estimation method for the DSB test is based on the assumption that the resultant horizontal strain increment is at all times zero, that is, an assumption that simple shear conditions exist in the shear band of the DSB test with the Mohr's circles of incremental strain and stress shown in Fig. 10 (Morgenstern and Tchalenko 1967; Rowe 1969; Wroth 1987; Dounias and Potts 1993; Shibuya et al. 1997). In the DSB test, the angle of shearing resistance is usually defined by  $\phi_{ds} = \tan^{-1} (\tau_{zx}/\sigma_z)$ , where  $\tau_{zx}$  and  $\sigma_z$  are the horizontal shear and vertical normal stresses on the horizontal plane, respectively. As can be seen in Fig. 10b, the angle of shearing resistance on the plane of maximum stress obliquity defined by  $\phi = \sin^{-1} [(\sigma_1 - \sigma_3)/(\sigma_1 + \sigma_3)]$  does not coincide with  $\phi_{ds}$  on the horizontal plane, suggesting that the horizontal failure plane in the DSB test is not the plane of maximum stress obliquity.

This issue is then investigated by using the DEM simulation results. Figure 12 shows the interparticle contact forces network in the simulated DSB test. The stresses in the DSB test can be calculated from the interparticle contact forces as follows (Christoffersen et al. 1981):

$$[7] \quad \sigma_{ij} = \left( \sum_R l_i F_j \right) / V$$

where  $R$  is the calculation domain;  $V$  is the volume of the domain;  $l$  is the length of vectors connecting the centers of contacting particles; and  $F_j$  is the contact force. As schematically shown in Fig. 13, we define the angle  $\beta$  as the inclination of the major principal stress ( $\sigma_1$ ) computed from the interparticle contact forces on the horizontal plane. Theo-

Fig. 13. Inclination of principal major stress ( $\sigma_1$ ) from interparticle contact forces.



retically, the angle between the major principal stress ( $\sigma_1$ ) and the plane of maximum stress obliquity is  $45^\circ - (\phi_{mo}/2)$ , in which  $\phi_{mo}$  is the mobilized friction angle. Figure 14 shows the distribution of the inclination angle  $\beta$  along the horizontal plane at the peak state (shear displacement  $D = 6.5$  mm). Because the failure in the DSB test occurs within the shear band, the calculation of the stresses from the interparticle contact forces, using eq. [7], is limited within the shear band. It is seen that for a large proportion of the sample, the inclination angle  $\beta$  is larger than  $45^\circ - (\phi_{mo}/2)$ . Furthermore, this finding also holds true during the shearing process, as shown in Fig. 15. In the simulated case, the difference between the angle of the plane of maximum stress obliquity and the angle of the horizontal failure plane is about  $5^\circ - 6^\circ$ .

Provided that the direction of the major principal strain increment ( $d\epsilon_1$ ) is inclined by  $45^\circ - (v/2)$  to the horizontal and that the direction of  $\sigma_1$  coincides with that of  $d\epsilon_1$  at failure, the relationship between  $\phi$  and  $\phi_{ds}$  is given by the following equation (Davis 1968) (see Fig. 10):

$$[8] \quad \tan \phi_{ds} = \sin \phi \cos v / (1 - \sin \phi \sin v)$$

**Fig. 14.** Inclination of major principal stress ( $\beta$ ) along the separation (horizontal) plane, at  $D = 6.5$  mm.

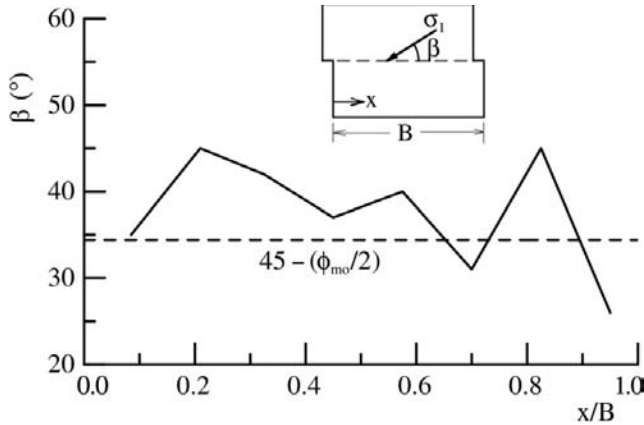


**Fig. 15.** Inclination of major principal stress during shear.

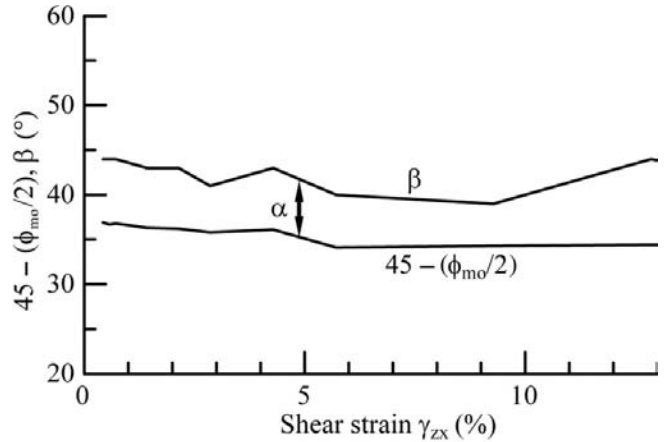
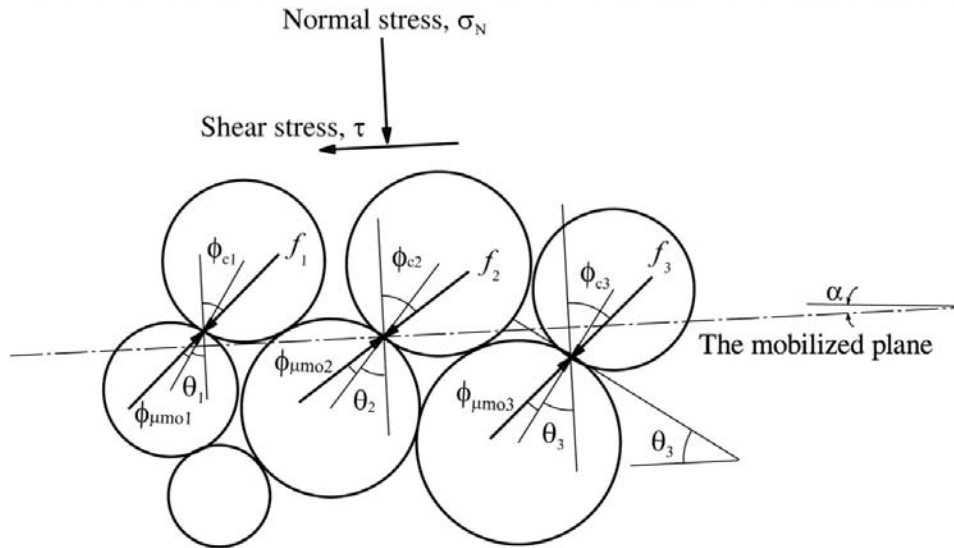


**Fig. 16.** Equilibrium for interparticle contact forces on the mobilized plane.



According to eq. [8], the value of  $\phi_{ds}$  is less than the value of  $\phi$ . Usually, the shear strength in the DSB test is computed on the horizontal plane (i.e.,  $\phi_{ds}$ ), which is thus considered to be on the safe side for the purposes of design.

**Microscopic interpretation of angle of shearing resistance for granular material**

Paying attention to the interparticle contacts along a mobilized plane (the plane of maximum stress obliquity at a given stress state) as shown in Fig. 16 and denoting the interparticle contact angle by  $\theta_i$ , the interparticle contact force by  $f_i$ , and the mobilized interparticle friction angle by  $\phi_{\mu moi}$ , one can obtain the following equation from the equilibrium of interparticle forces on the mobilized plane:

$$[9] \quad \frac{\tau}{\sigma_N} = \frac{\sum_{i=1}^n f_i \sin(\theta_i + \phi_{\mu moi})}{\sum_{i=1}^n f_i \cos(\theta_i + \phi_{\mu moi})} = \frac{\sum_{i=1}^n f_i \sin \phi_{ci}}{\sum_{i=1}^n f_i \cos \phi_{ci}}$$

where  $n$  is the number of the interparticle contacts along the mobilized plane; and  $\phi_{ci}$  (subscript “c” denotes “contact”) is the angle between the interparticle contact force ( $f_i$ ) and the normal to the mobilized plane. In this paper, the angle  $\phi_{ci}$  ( $= \theta_i + \phi_{\mu moi}$ ), varying from  $-\pi/2$  to  $\pi/2$ , is defined for convenience as the angle of interparticle force.

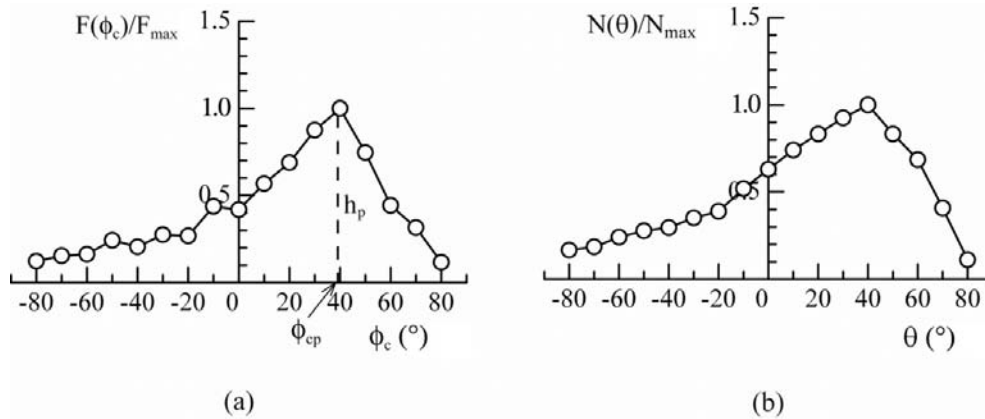
Along the mobilized plane, all the interparticle forces ( $f_i$ ) can be characterized by a probability distribution function with respect to the angle  $\phi_{ci}$ , denoted as  $F(\phi_c)$ . Figure 17a shows the normalized distribution of  $F(\phi_c)$  in the shear zone corresponding to those shown in Figs. 8 and 12. It is found that the normalized  $F(\phi_c)$  takes approximately a triangular distribution, which can be expressed as

$$[10a] \quad F(\phi_c) = \frac{h_p(\phi_c + \pi/2)}{\phi_{cp} + \pi/2} \quad (-\pi/2 \leq \phi_c \leq \phi_{cp})$$

$$[10b] \quad F(\phi_c) = \frac{h_p(\phi_c - \pi/2)}{\phi_{cp} - \pi/2} \quad (\phi_{cp} \leq \phi_c \leq \pi/2)$$

where  $h_p$  and  $\phi_{cp}$  are the height and the corresponding angle of interparticle force at the peak of the triangular distribu-

**Fig. 17.** Triangular probability distributions of (a) interparticle contact forces,  $F(\phi_c)$ , and (b) interparticle contact angles,  $N(\theta)$ , on the mobilized plane.



tion, respectively. Replacing  $f_i$  in eq. [9] approximately with  $F(\phi_c)$  and integrating over the angle range, one can get

$$[11] \quad \frac{\tau}{\sigma_N} = \frac{\int_{-\pi/2}^{\pi/2} F(\phi_c) \sin \phi_c d\phi_c}{\int_{-\pi/2}^{\pi/2} F(\phi_c) \cos \phi_c d\phi_c} = \tan 3\bar{\phi}_c - \frac{6\bar{\phi}_c}{\pi \cos 3\bar{\phi}_c}$$

where

$$[12] \quad \bar{\phi}_c = \frac{\sum_{i=1}^n f_i \phi_{ci}}{\sum_{i=1}^n f_i} = \frac{\sum_{i=1}^n f_i (\theta_i + \phi_{\mu moi})}{\sum_{i=1}^n f_i}$$

$$= \frac{\sum_{i=1}^n f_i \theta_i}{\sum_{i=1}^n f_i} + \frac{\sum_{i=1}^n f_i \phi_{\mu moi}}{\sum_{i=1}^n f_i}$$

$$= \frac{\int_{-\pi/2}^{\pi/2} F(\theta) \theta d\theta}{\int_{-\pi/2}^{\pi/2} F(\theta) d\theta} + \frac{\int_{-\pi/2}^{\pi/2} F(\theta) \phi_{\mu mo}(\theta) d\theta}{\int_{-\pi/2}^{\pi/2} F(\theta) d\theta}$$

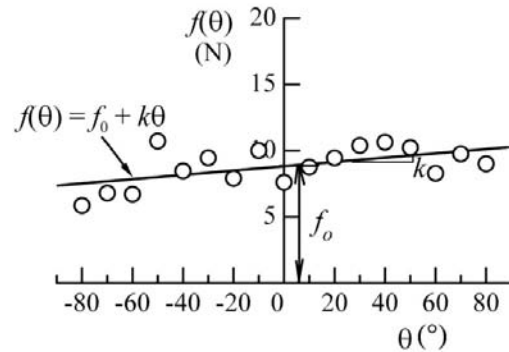
$$= \bar{\phi}_c(\theta) + \bar{\phi}_c(\phi_{\mu mo})$$

in which  $F(\theta)$  and  $\phi_{\mu mo}(\theta)$  are the probability distribution of interparticle contact forces and the mobilized interparticle friction angle with respect to the contact angle  $\theta$  along the mobilized plane, respectively. As is apparent, the angle  $\bar{\phi}_c$  is the average angle of the interparticle forces weighted by  $F(\theta)$ .

Figure 17b shows the distribution of the contact numbers with respect to the contact angle  $\theta$ , designated as  $N(\theta)$ , along the mobilized plane in accordance with Fig. 17a. Similarly, it can also be approximated with a triangular distribution. The average interparticle contact angle ( $\bar{\theta}$ ) is calculated by

$$[13] \quad \bar{\theta} = \frac{\int_{-\pi/2}^{\pi/2} N(\theta) \theta d\theta}{\int_{-\pi/2}^{\pi/2} N(\theta) d\theta}$$

**Fig. 18.** Linear probability distribution of the average interparticle contact forces plotted using the data in Fig. 17.



From Fig. 17, one can compute the distribution of the average interparticle force,  $f(\theta)$ , which is shown in Fig. 18. Generally speaking, the interparticle contact force has a higher value along the shearing direction ( $\theta > 0$ ) than against it ( $\theta < 0$ ) (also see Fig. 12). The average interparticle force  $f(\theta)$  can be fitted linearly as

$$[14] \quad f(\theta) = f_0 + k\theta$$

where  $k$  is the slope of the straight line for  $f(\theta)$ ; and  $f_0 = f(0)$  is taken as the average within the range  $-\pi/2$  to  $\pi/2$ . It is seen that  $f(\theta)$  is biased (favorable) toward the shearing direction with  $k > 0$  and becomes an even distribution ( $k = 0$ ) if the contact force at each contact was assumed to be constant.

For a specific contact angle ( $\theta$ ), the total interparticle contact force,  $F(\theta)$ , is the product of the average interparticle force  $f(\theta)$  and the number of the contacts  $N(\theta)$ , as shown in Fig. 19. It is expressed as

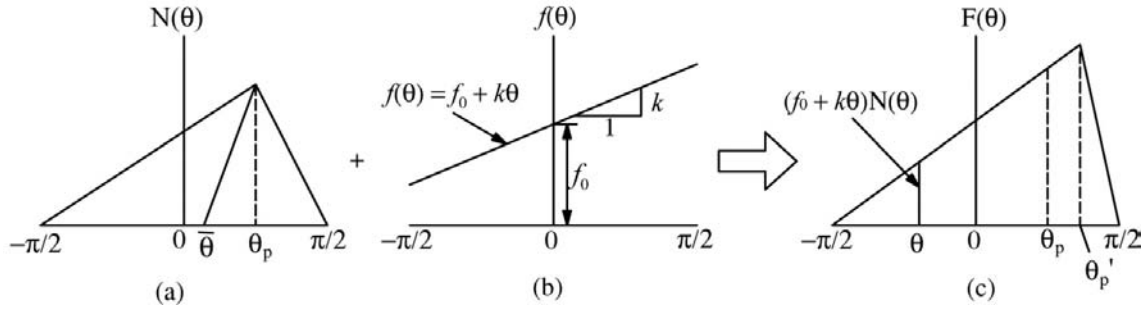
$$[15] \quad F(\theta) = f(\theta)N(\theta) = (f_0 + k\theta)N(\theta)$$

Replacing  $F(\theta)$  in eq. [12] with eq. [15], we have

$$[16a] \quad \bar{\phi}_c \cong \bar{\theta} + \frac{k}{f_0} \left( 1.5\bar{\theta}^2 + \frac{\pi^2}{24} \right) = \bar{\theta} + \delta$$

$$[16b] \quad \delta = \frac{k}{f_0} \left( 1.5\bar{\theta}^2 + \frac{\pi^2}{24} \right)$$

**Fig. 19.** Composition of the probability distribution of the total contact forces on the mobilized plane: (a) probability distribution of the contact angles; (b) probability distribution of the average contact forces; (c) probability distribution of the total contact forces.



The reader may refer to Liu and Matsuoka (2001, 2003) for the implementation details.

Figure 20 shows the evolution of the statistically microscopic variables  $\bar{\phi}_c$  and  $\bar{\theta}$  during the shearing process of the simulated DSB test (for simplicity,  $\bar{\phi}_c$  and  $\bar{\theta}$  are analyzed on the horizontal plane). The difference (angle  $\delta$ ) between these two variables varies slightly when  $\gamma_{zx} > 1\%$ . A similar trend has also been exhibited in the SSTs on different samples and in the in situ DSB tests on various granular materials (Liu and Matsuoka 2001, 2003). Thus, the difference angle ( $\delta$ ) may be assumed to be constant during shear except for small strains.

As the mobilized angle of internal friction of granular material is commonly defined as  $\phi = \tan^{-1}(\tau/\sigma_N)$ , it is understood from eqs. [11] and [16] that  $\phi$  is related to the average contact angle ( $\bar{\theta}$ ) and the ratio  $k/f_0$  representing the degree of the probability distribution of the interparticle contact forces that is biased toward the positive zone of the contact angle ( $\theta$ ) (along the shearing direction). It may be recognized that the shear strength need not necessarily change if the interparticle friction ( $\phi_\mu$ ) varies. In other words, the internal friction angle ( $\phi$ ) of granular material does not directly relate to the interparticle friction angle ( $\phi_\mu$ ). This argument is contrary to what is usually recognized for the shear strength (or the internal friction angle,  $\phi$ ) of granular materials (e.g., Lee and Seed 1967; Matsuoka and Yamamoto 1994), but it agrees with the discussions by Skinner (1969), Walton and Braun (1986), Cambou et al. (1993), and Oger et al. (1998), who found that the global internal friction angle ( $\phi$ ) increases with the interparticle angle ( $\phi_\mu$ ) at a very small value of  $\phi_\mu$  but is essentially constant for a larger  $\phi_\mu$  value.

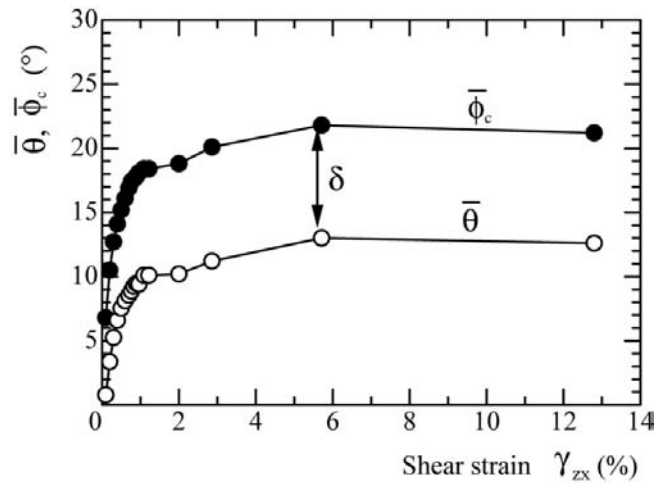
### Microscopic interpretation of a stress-dilatancy relationship for granular material

Matsuoka (1974) correlated the ratio of the normal strain increment to the shear strain increment,  $-d\varepsilon_N/d\gamma$ , with the probability distribution,  $N(\theta)$ , of interparticle contact angles along the mobilized plane as follows:

$$[17] \quad -\frac{d\varepsilon_N}{d\gamma} = \frac{\int_{-\pi/2}^{\pi/2} N(\theta) \sin \theta d\theta}{\int_{-\pi/2}^{\pi/2} N(\theta) \cos \theta d\theta}$$

As mentioned above,  $N(\theta)$  can be approximated with a triangular distribution (Fig. 17b). Substituting the triangular

**Fig. 20.** Evolution of the microscopic quantities  $\bar{\phi}_c$ ,  $\bar{\theta}$ , and  $\delta$  in the shear band during the shear process.



distribution into the right-hand side of eq. [17] and integrating it, we get

$$[18] \quad -\frac{d\varepsilon_N}{d\gamma} = \tan 3\bar{\theta} - \frac{6\bar{\theta}}{\pi \cos 3\bar{\theta}}$$

Associated with eqs. [11], [16], and [18], the relationship between the shear stress to normal stress ratio ( $\tau/\sigma_N$ ) and the normal strain increment to shear strain increment ratio ( $-d\varepsilon_N/d\gamma$ ), that is, the stress-dilatancy relationship, is through three microstructural parameters,  $\bar{\phi}_c$ ,  $\bar{\theta}$ , and  $\delta$ , where the angle  $\delta$  is assumed to be constant during shear as mentioned earlier.

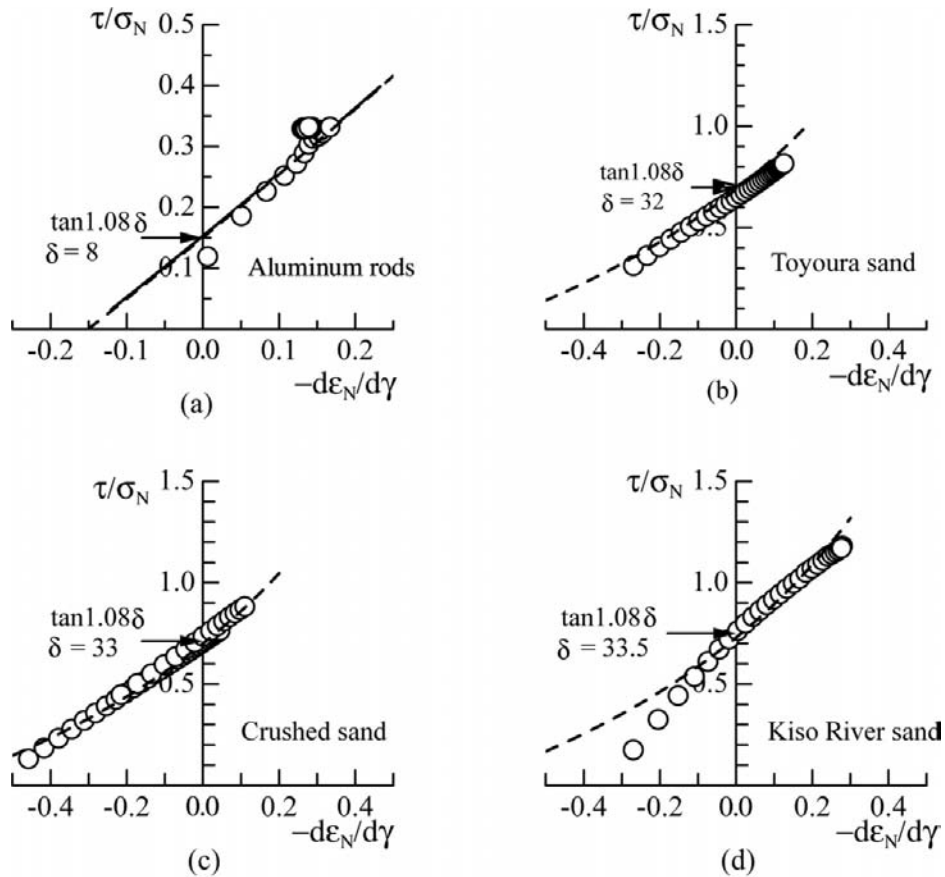
Corresponding to the possible ranges of  $\bar{\phi}_c \leq 50^\circ$  for common granular soils, the value of  $\tan 3\bar{\phi}_c - [6\bar{\phi}_c/(\pi \cos 3\bar{\phi}_c)]$  varies from  $\tan 1.09\bar{\phi}_c$  to  $\tan 1.07\bar{\phi}_c$ . Equation [11] is thus converted to

$$[19] \quad \frac{\tau}{\sigma_N} = \tan 3\bar{\phi}_c - \frac{6\bar{\phi}_c}{\pi \cos 3\bar{\phi}_c} \cong \tan 1.08 \bar{\phi}_c$$

Likewise, eq. [18] is converted to

$$[20] \quad -\frac{d\varepsilon_N}{d\gamma} = \tan 3\bar{\theta} - \frac{6\bar{\theta}}{\pi \cos 3\bar{\theta}} \cong \tan 1.08 \bar{\theta}$$

**Fig. 21.** Microscopically based stress–dilatancy relationships (lines) and experimental results (plots).



Subsequently, the explicit expression of the stress–dilatancy relationship through eqs. [11], [16], and [18] may be converted to

$$[21] \quad \frac{\tau}{\sigma_N} = \lambda \left( -\frac{d\epsilon_N}{d\gamma} \right) + \mu$$

where

$$[22] \quad \lambda = \frac{1 + \tan^2 1.08\delta}{1 - \tan 1.08\delta \left( -\frac{d\epsilon_N}{d\gamma} \right)} \text{ and } \mu = \tan 1.08\delta$$

It is apparent that eq. [21] is the same expression as proposed by Matsuoka (1974), but the parameters have a different physical significance. The parameters  $\lambda$  and  $\mu$  are functions of  $\delta$  dependent on the interparticle microstructures: the average contact angle ( $\bar{\theta}$ ) and the distribution of the interparticle contact forces during shearing deformation (dominant along the shear direction).

For the simulated DSB test, the average value of  $\delta$  during the shearing process is about  $8^\circ$ . Microscopically, the stress–dilatancy relation calculated with  $\delta = 8^\circ$  through eqs. [11], [16], and [18] (solid line) and through eq. [21] (dashed line) are plotted in Fig. 21a. Meanwhile, from the macroscopic point of view, the measurable stress–dilatancy relation obtained in the simulated DSB test is marked in Fig. 21a as well, with circles. These values appear to be very consistent. Furthermore, for other granular field materials, such as

Toyourea sand (0.10–0.30 mm diameter;  $e_0 = 0.71$ ), crushed sand (0.42–2.0 mm diameter;  $e_0 = 0.82$ ), and Kiso River sand (0.07–2.0 mm diameter;  $e_0 = 1.03$ ), the average value of  $\delta$  during shear ranges from  $32^\circ$  to  $37^\circ$  (Liu and Matsuoka 2003). The stress–dilatancy relations from the proposed method are accordingly marked in Figs. 21b–21d. The agreements are obvious as well. Therefore, eqs. [11], [16], and [18] or eq. [21] excellently explain the stress–dilatancy relationship of granular materials on the mobilized plane quantitatively allied with the microscopic and macroscopic behaviors.

### Conclusions

In this paper, the intrinsic drawbacks involved in performing and interpreting conventional DSB tests have been identified through DEM simulations. The angle of internal friction and a stress–dilatancy relationship for granular material are interpreted from a microscopic view of point.

In the conventional DSB test where the vertical movement of the upper shear box is restrained, the measurement of the average normal stress on the horizontal plane involves a frictional force developed between the inside surface of the upper shear box and the sample, which is downward for the dense sample (dilatant sample) and upward for the loose sample (contractive sample). As a result, the shear strength is overestimated for the dense sample and underestimated for the loose sample in the conventional DSB test. The influences of this interface frictional force can be minimized or

even eliminated if the upper shear box is allowed to move freely in the vertical direction or the normal force is measured on the side opposite the loading plate.

In the DSB test, a thin soil element at mid-height is subjected to simple shear deformation. Given the thickness of this deformation, the shear and the normal strains on the horizontal plane can be readily estimated; these can in turn be converted into the principal strains and are extendable to 3D. The experimental validations clearly indicate that the proposed strain estimation method is rational; thus, the DSB test may be used to establish the constitutive relationship for granular materials as well.

The internal friction angle ( $\phi$ ) for granular material is related to the statistically microscopic value  $\bar{\phi}_c$  by eq. [11], where  $\bar{\phi}_c$  is the sum of the average contact angle ( $\bar{\theta}$ ) and the angle  $\delta$ . The angle  $\delta$  depends on the interparticle microstructures: the average contact angle ( $\bar{\theta}$ ) and the ratio  $k/f_0$ , characterized by a probability distribution of the average interparticle contact forces that is biased toward the positive zone of the contact angle  $\theta$  (along the shear direction). For most granular materials, the angle  $\delta$  depends weakly on the interparticle friction angle ( $\phi_\mu$ ) except when  $\phi_\mu$  has very low values.

The stress–dilatancy relationship of granular material based on the mobilized plane, that is, the relationship between the shear stress to normal stress ratio ( $\tau/\sigma_N$ ) and the normal strain increment to shear strain increment ratio ( $-d\varepsilon_N/d\gamma$ ) can be correlated to three microscopic variables,  $\bar{\phi}_c$ ,  $\bar{\theta}$ , and  $\delta$  through eqs. [11], [16], and [18] or eq. [21].

Finally, it is pointed out that in this paper, the more reasonable derivations for eqs. [11] and [18] have been achieved by using the two triangular distributions of  $F(\phi_c)$  and  $N(\theta)$ , resulting in  $\mu = \tan 1.08\delta$ .

## Acknowledgements

The author is grateful to Prof. H. Matsuoka of the Nagoya Institute of Technology for his great support and valuable discussions. Very special thanks go to Dr. H. Chen (Golder Associates Ltd.) for her help with the English language.

## References

- Bolton, M.D. 1986. The strength and dilatancy of sands. *Géotechnique*, **36**(1): 65–78.
- Cambou, B., Sidoroff, F., Mahboubir, A., and Dubujet, P.H. 1993. Distribution of micro variables in granular media, consequences on the global behaviour. *In Modern Approaches to Plasticity: Proceedings of a Workshop*, Horton, Greece, 12–16 June 1992. Edited by D. Kolymbas. Elsevier Science Publisher, Amsterdam, The Netherlands. pp. 199–212.
- Christoffersen, J., Mehrabadi, M.M., and Nemat-Nasser, S. 1981. A micromechanical description of granular material behavior. *Journal of Applied Mechanics*, ASME, **48**(2): 339–344.
- Cole, E.R. 1967. The behaviour of soil in the simple shear apparatus. Ph.D. thesis, University of Cambridge, Cambridge, UK.
- Cundall, P.A. 1971. A computer model for simulating progressive, large-scale movements in blocky rock systems. *In Rock Fracture: Proceedings of a Symposium of the International Society of Rock Mechanics*, Nancy, France. Vol. 2, pp. 129–136.
- Cundall, P.A., and Strack, O.D.L. 1979. A discrete numerical model for granular assemblies. *Géotechnique*, **29**(1): 47–65.
- Davis, E.H. 1968. Theories of plasticity and the failure of soil masses. *In Soil mechanics: selected topics*. Edited by I.K. Lee. Butterworth, London, UK. pp. 341–380.
- Dounias, G.T., and Potts, D.M. 1993. Numerical analysis of drained direct and simple shear tests. *Journal of Geotechnical Engineering*, ASCE, **119**(12): 1870–1891.
- Dyer, M.R. 1986. Observation of the stress distribution in crushed glass with applications to soil reinforcement. Ph.D. thesis, University of Oxford, Oxford, UK.
- Japanese Geotechnical Society. 1997. Method for consolidated constant pressure direct shear box test on soils. *Tsuchi-to-Kiso*, **45**(1): 70–74. [In Japanese.]
- Lee, K.L., and Seed, H.B. 1967. Drained strength characteristics of sands. *Journal of the Soil Mechanics and Foundations Division*, ASCE, **93**(SM6): 117–141.
- Lings, M.L., and Dietz, M.S. 2004. An improved direct shear apparatus for sand. *Géotechnique*, **54**(4): 245–256.
- Liu, S.H. 1999. Development of a new direct shear test and its application to the problems of slope stability and bearing capacity. Ph.D. thesis, Nagoya Institute of Technology, Nagoya, Japan.
- Liu, S.H., and Matsuoka, H. 2001. A microscopic study on stress–dilatancy relationship of granular material by DEM. *In Powders and Grains 2001: Proceedings of the 4th International Conference on Micromechanics of Granular Media*, Sendai, Japan. 21–25 May 2001. A.A. Balkema, Rotterdam, The Netherlands. pp. 207–211.
- Liu, S.H., and Matsuoka, H. 2003. Microscopic interpretation on a stress–dilatancy relationship of granular materials. *Soils and Foundations*, **43**(3): 73–84.
- Masson, S., and Martinez, J. 2001. Micromechanical analysis of the shear behavior of a granular material. *Journal of Engineering Mechanics*, ASCE, **127**(10): 1007–1016.
- Matsuoka, H. 1974. Stress–strain relationships of sands based on the mobilized plane. *Soils and Foundations*, **14**(2): 45–61.
- Matsuoka, H. 1983. Deformation and strength of granular materials based on the theory of “compounded mobilized planes” (CMP) and “spatial mobilized plane” (SMP). *In Advances in the mechanics and the flow of granular materials*. Edited by M. Shahinpoor. Gulf Publishing Company, Houston, Tex., Vol. 2, pp. 813–836.
- Matsuoka, H., and Yamamoto, S. 1994. A microscopic study on shear mechanism of granular materials by DEM. *Journal of Geotechnical Engineering*, JSCE, **487**(III-26): 167–175. [In Japanese.]
- Matsuoka, H., Liu, S.H., Satoh, S., Shibahara, K., Nishikata, U., and Ijiri, K. 1999. Estimation of strains in direct shear test. *In Proceedings of the 54th Annual Conference of the Japan Society of Civil Engineering*. Part III-A18. [In Japanese.]
- Matsuoka, H., Sun, D.A., Liu, S.H., Nishikata, U., and Teramoto, S. 2001. Simple improvements on existing direct box shear apparatus of small and large sizes. *Tsuchi-to-Kiso*, **49**(1): 21–24. [In Japanese.]
- Morgenstern, N.R., and Tchalenko, J.S. 1967. Microscopic structures in kaolin subjected to direct shear. *Géotechnique*, **17**: 309–328.
- Oger, L., Savage, S.B., Corriveau, D., and Sayed, M. 1998. Yield and deformation of an assembly of disks subjected to a deviatoric stress loading. *Mechanics of Materials*, **27**: 189–210.
- Rowe, P.W. 1969. The relation between the shear strength of sands in triaxial compression, plane strain and direct shear. *Géotechnique*, **19**(1): 75–86.
- Shibuya, S., Mitachi, T., and Tamate, S. 1997. Interpretation of direct shear box testing of sands as quasi-simple shear. *Géotechnique*, **47**(4): 769–790.

- Skempton, A.W., and Bishop, A.W. 1950. The measurement of the shear strength of soils. *Géotechnique*, **2**: 98.
- Skinner, A.E. 1969. A note on the influence of interparticle friction on the shearing strength of a random assembly of spherical particles. *Géotechnique*, **19**(1): 150–157.
- Sumi, T., Oshima, A., Takada, N., and Fukami, T. 1997. Effect of specimen thickness of split box shear test under constant pressure condition (2). *In Proceedings of the 52th Annual Conference of the Japan Society of Civil Engineering. Part III-A30*, pp. 60–61. [In Japanese.]
- Takada, N., Oshima, A., and Sakamoto, Y. 1996. Effect of specimen thickness of split box shear test under constant pressure condition. *In Proceedings of the 31st Japan National Conference on Geotechnical Engineering*, pp. 669–670. [In Japanese.]
- Taylor, D.W. 1948. *Fundamentals of soil mechanics*. John Wiley & Sons, New York.
- Thornton, C. 2000. Numerical simulations of deviatoric shear deformation of granular media. *Géotechnique*, **50**(1): 43–53.
- Thornton, C., and Zhang, L. 2001. A DEM comparison of different shear testing devices. *In Powders and Grains 2001: Proceedings of the 4th International Conference on Micromechanics of Granular Media*, Sendai, Japan, 21–25 May 2001. A.A. Balkema, Rotterdam, The Netherlands. pp. 183–190.
- Walton, O.R., and Braun, R.L. 1986. Viscosity, granular-temperature, and stress calculations for shearing assemblies of inelastic, frictional disks. *Journal of Rheology*, **50**(5): 949–980.
- Wroth, C.P. 1987. The behavior of normally consolidated clay as observed in undrained direct shear tests. *Géotechnique*, **37**(1): 37–43.
- Yamamoto, S. 1995. *Fundamental study on mechanical behavior of granular materials by DEM*. Ph.D. thesis, Nagoya Institute of Technology, Nagoya, Japan. [In Japanese.]